JOURNAL OF MATERIALS SCIENCE 5 (1970) 171-181

The Application of Differential Thermal Analysis by High Temperature Microscopy to Kinetic and Structural Studies on the Crystallisation of Glasses

D. CLINTON, R. A. MERCER, R. P. MILLER
National Physical Laboratory, Teddington, Middx, UK

The application of a recently developed micro differential thermal analyser (μDTA) to studies on the crystallisation of glasses is described.

The technique permits continuous visual observation of microdroplets of melts and glasses during thermal analysis over a wide range of heating and cooling rates.

Nucleation and crystallisation processes can be studied in conjunction with techniques of X-ray diffraction and electron microscopy. Crystal growth rates can be measured. Semiquantitative values for the heats of crystallisation of glasses can be obtained and kinetic data relating to the rate at which glasses undergo volume crystallisation can be derived from an analysis of the thermograms.

The scope of the technique in linking structural information with the thermal and kinetic data associated with transformations in glasses is illustrated with data from three lithium aluminosilicate glasses.

1. Introduction

The usefulness of differential thermal analysis (DTA) as a method of monitoring and defining thermal effects accompanying chemical changes and structural transformations is well known. A continuous record is obtained of the differential temperature ($\triangle T$) existing between a sample and a thermally inert reference sample when both undergo an identical, constant rate of temperature increase. A simultaneous record of the sample temperature is also normally made.

In principle such thermograms can be used to determine both the heat of reaction and the reaction kinetics, but success in such determinations has been limited by the difficulties in formalising the factors responsible for the $d\triangle T/dt$ peaks. Peak shape has been shown [1] to be a function not only of the reaction kinetics and energetics but also of the heating rate and the geometry and thermal diffusivities within the furnace, specimen, standard, and thermocouple assembly.

In this paper, attention is drawn to the use of a recently developed μDTA apparatus [2] in which the use of thermocouples as both heaters and sample holders greatly simplifies analysis of the peaks. A secondary but important result of this unique design is that samples can be quenched very rapidly, thus enabling more direct associations to be drawn between observed heat effects and the microstructure and crystalline state of the sample. The design allows faster heating and cooling rates than is normally possible and the small sample size results in good resolution of peaks.

The microscopic dimensions of the samples ensure that temperature uniformity is good, and lead to the rapid establishment of chemical and thermal equilibrium and fast response to heat effects.

The sample holder is mounted in a draught-proof cell on the stage of a polarising microscope, thus permitting continuous observation and photomicrography of specimens during heating or cooling. Examples will be given of the application of μDTA to studies on the crystallisation of some lithium aluminosilicate glasses.

TABLE I Glass compositions

Glass no.	Li_2O mole ratio	Li_2O wt %	Al_2O_3 mole ratio	Al_2O_3 wt %	SiO_2 mole ratio	SiO_2 wt %	TiO_2 mole ratio	TiO_2 wt %
G66	34.47	19.46	7.76	14.96	57.76	65.68	—	—
G69	34.47	17.48	7.74	13.44	57.76	58.91	7.5	10.17
G70	37.26	18.92	8.39	14.55	54.34	55.51	8.11	11.01

2. Experimental

2.1. Glass Compositions

The compositions of the three glasses examined are given in table I. G66 corresponds in composition to the eutectic which occurs between β-spodumene (54.6 wt %) and lithium metasilicate (45.4 %). G69 has the same $Li_2O : Al_2O_3 : SiO_2$ ratio with 7.5 moles of TiO_2 added on the basis of $Li_2O + Al_2O_3 + SiO_2 = 100$ moles, whereas in G70, 7.5 moles of TiO_2 replace the equivalent molar quantity of SiO_2.

Full details of the preparation and properties of these glasses have been given elsewhere [3].

2.2. The μDTA Instrument

Previous papers [4, 5, 6, 12] have described the apparatus and general techniques of hot stage microscopy based on directly heated thermocouple sample supports. The use of twin thermocouple supports capable of measuring both the sample temperature and the differential temperature has also been described elsewhere [2, 13].

2.3. Crystal Growth Rates

Crystal growth rates were determined only on G66 and G69 since it was difficult to identify individual crystals in G70. Growth-rate measurements were made by quenching, at timed intervals, a series of beads which had had identical programmed heating to a given temperature. The crystal sizes were measured by transmission optical microscopy of polished thin-sections of the beads. Time lapse photography, which would frequently be possible, was ruled out in the case of these glasses because of surface crystallisation.

2.4. X-ray Diffraction

Crystal phase identification was made by X-ray powder diffraction on quenched beads.

2.5. Electron Microscopy

Techniques have been developed whereby the microstructure of quenched beads can be examined by electron microscopy both by replication and transmission methods.

For replication, resin-embedded samples were polished and etched, carbon and platinum were evaporated simultaneously on to the surface and the replica was floated on to a copper grid. Fortuitous adherence of crystalline inclusions frequently made possible selected area diffraction. Samples for transmission study were prepared by cutting thin sections of similarly embedded samples with a diamond knife in an LKB ultramicrotome.

2.6. Enthalpic Calibration of the Apparatus

The relationship between peak area and heat of reaction (fig. 1) was determined for the apparatus by measurement of thermograms from weighed quantities of lithium sulphate, potassium sulphate and sodium chloride. Sample weights ranged between 100 and 900 μg.

The relevant reactions were the solid state transitions occurring at 560° C in Li_2SO_4 ($\triangle H = 6.5$ kcal mol^{-1}) and at 583° C in K_2SO_4 ($\triangle H = 1.94$ kcal mol^{-1}) and the fusion of NaCl at 800° C ($\triangle H = 7.83$ kcal mol^{-1}).

It was found that strict proportionality between peak area and heat of reaction held over only a relatively narrow sample weight range. This is considered to be due to the fact that larger samples cause disproportionate losses of heat along the thermocouple wires away from the thermojunction.

The heats of crystallisation of the three glasses, recorded in table II, are mean values derived from several analyses on each glass using sample weights ranging from 350 to 950 μg and heating rates of 3.75 and 7.5° C sec^{-1}.

3. Thermocouple Assembly Characteristics

To formalise some of the advantages offered by using this type of assembly, reference can be made to fig. 2 which represents the temperature relationship between a sample and a reference

TABLE II Thermal and crystallisation rate data during μDTA of glasses G66, G69, and G70; heating rate 3.6° C sec^{-1}

Glass	T_g, °C	Exotherm temperature range, °C	Phases crystallising	Heat of crystallisation, cals g^{-1}	Rate of volume crystallisation at 750° C, % sec^{-1}	Apparent activation energy of volume crystallisation, kcal mol^{-1}
G66	520	710 to 840	Li_2SiO_3 β-eucryptite ss	75	2.3	79 ± 10
G69	530	710 to 810	Li_2SiO_3 β-eucryptite ss $LiTiO_3$	74	3.0	103 ± 15
G70	510	710 to 780	Li_2SiO_3 β-eucryptite ss $LiTiO_3$	82	6.0	146 ± 10

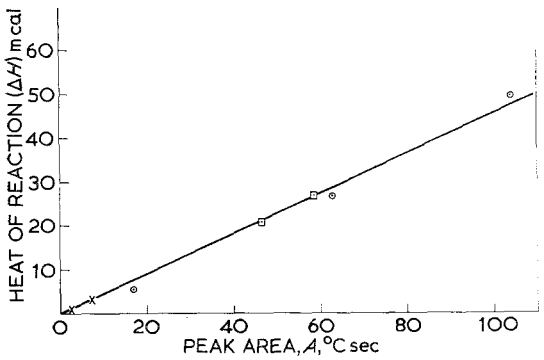

Figure 1 Enthalpic calibration of μDTA (0.3 mm diameter thermocouples). ○, Li_2SO_4; X, K_2SO_4; ⊡, NaCl; $K = \Delta H/A$ = 0.45 mcal ° C^{-1} sec^{-1}.

material during the DTA of a hypothetical endothermic process occurring at temperature T_m.

If K is a temperature-normalising coefficient between the sample and the reference material, r is the heating rate, T_r is the temperature of the reference junction, T_s is the temperature of the sample junction, $\triangle T = T_r - T_s$, C_p is the heat content of the sample and its support, and $\triangle H$ is the amount of heat associated with the reaction, then, making the usual assumption that C_p and K are independent of temperature over the interval involved, during a time period dt when the reaction is occurring the heat balance equation is

$$C_p d\triangle T = d\triangle H - K\triangle T dt . \quad (1)$$

If t_1 and t_2 are the times at the beginning and end of a peak then it follows from equation 1 that

$$\triangle H = K\int_{t_1}^{t_2} \triangle T dt \quad (2)$$

$$= K \text{ peak area } (A). \quad (3)$$

K is obtained from measured peak areas.

K is a function of sample, cell, and furnace geometry and is frequently complicated by factors such as specimen shrinkage and temperature non-uniformity arising from problems of thermal transfer. These disadvantages largely disappear in the study of glasses with the present apparatus and equation 2 becomes more valid.

The experimentally determined value of K was 0.45 mcals° C^{-1}sec^{-1}.

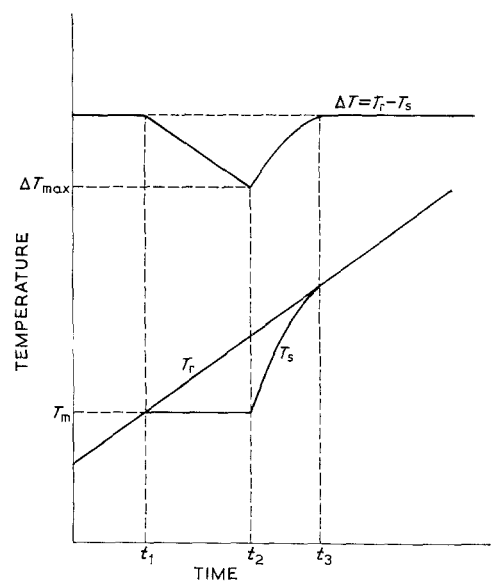

Figure 2 Idealised differential thermogram of an endothermic process. T_m, temperature at beginning of endotherm at time t_1; T_r, temperature of reference material; T_s, temperature of sample; t_2, time at which reaction is complete; t_3, time at which endotherm is complete.

Following from equation 1, between temperatures t_1 and t_2

$$\int_{t_1}^{t_2} K(T_1 - T_s)dt = \int_{t_1}^{t_2} Cp dT_s + \int_{t_1}^{t_2} d\triangle H . \quad (4)$$

Since

$$T_r = T_s + rt , \ (t_1 \leq t \leq t_2) , \quad (5)$$

$$\triangle T_{max} = r(t_2 - t_1) , \quad (6)$$

from equation 4

$$\frac{Kr(t_1 - t_1)^2}{2} = \triangle H \quad (7)$$

$$\triangle T_{max} = \sqrt{\frac{2r\triangle H}{K}} . \quad (8)$$

This equation shows that the reduction that might have been expected in $\triangle T_{max}$ from the use of small sample weights is offset by small values of K and the use of higher heating rates. The small value of K (0.45 mcals° $C^{-1}sec^{-1}$) also increases the validity of the method of deriving kinetic data from an analysis of the thermograms (cf. section 5.2).

With regard to heating rate, in conventional DTA, heating rates are usually standardised at 10° C min^{-1} and, although in other μDTA apparatus [7] rates of 80° C min^{-1} have been quoted, the present instrument is capable of operating at 200 to 300° C sec^{-1}. In the work reported here, however, such high heating rates were inappropriate and rates of between 2.75 and 7.5° C sec^{-1} were used.

For a typical glass sample of 500 μg (specific heat of glass ~0.25 cals° C^{-1} g^{-1}) in contact with 1 mm of 0.3 mm diameter platinum wire (sp. ht. Pt = 0.03 cals° C^{-1} g^{-1}, the total heat content is 0.17 mcals° C^{-1}. It is this low heat content of the microfurnace that enables quenching rates of the order 10^3 °C sec^{-1} to be achieved by switching off the heating current.

4. Structural Transformations During DTA of Glasses

The thermograms of the three glasses G66, G69 and G70 are compared in fig. 3. The glass transformation temperatures (T_g), at which there are sharp changes of specific heat, are indicated by endothermic base line shifts. Crystallisation is marked by the exothermic peaks, and from the variations in the crystallisation temperatures, peak spans and peak shapes it can be implied

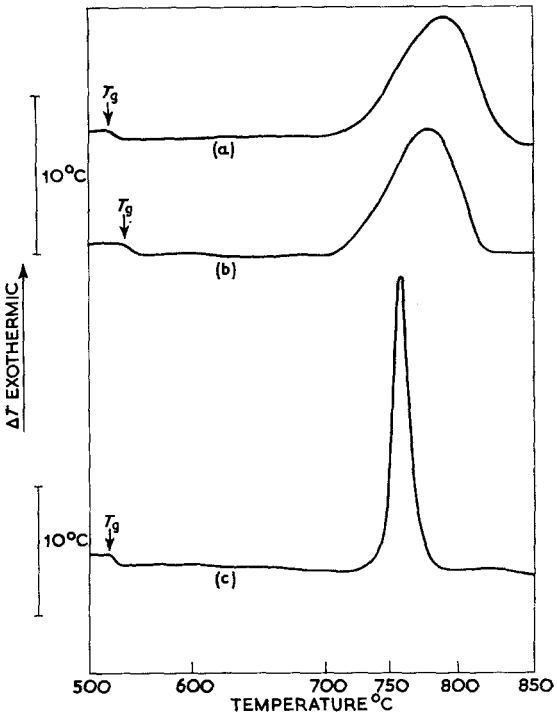

Figure 3 Crystallisation thermograms of glasses G66, G69 and G70. Heating rate 3.6° C sec^{-1}. T_g, glass transformation temperature; (a) G66, 950 μg; (b) G69, 660 μg; (c) G70, 420 μg.

qualitatively that there are differences in the processes of precipitation.

These differences have been discussed in detail in another paper [3] on the basis of results from studies on bulk quantities of these glasses. The following data which is derived solely from experiments on the hot stage μDTA apparatus generally corroborates the earlier findings and confirms the validity of observations on the micro scale. The derivation of kinetic parameters of the crystallisation process from the data will be described in later sections (5.1 and 5.2).

4.1. Observations on G66

Beads quenched after T_g but before the beginning of the exothermic peak were optically clear and replicas showed no structure in the electron microscope.

Visual observation showed that the exothermic effect was due to the formation of spherulites (fig. 4). The size and numbers of spherulites growing during DTA was independent of any precrystallisation heating. At the completion of the exotherm the spherulites had impinged to give

a coarse-grained microstructure and the bead remained translucent.

X-ray analysis of the beads quenched at several stages during their growth showed that the spherulites contained both lithium metasilicate and a β-eucryptite solid solution ($a = 5.19$, $c = 5.39$ Å). Extraction replication of spherulites from which the lithium metasilicate had been leached by etching with HF, showed that the β-eucryptite phase grows in the spherulites as radiating filaments (fig. 5).

At 900° C, just prior to the onset of fusion, the beads became optically opaque. The change was unaccompanied by any sensible heat effect. X-ray analysis showed that there had been no change in the phases present but electron micrographs revealed that internal recrystallisation had occurred in the spherulite domains to give a microstructure consisting of a regular dispersion of micron sized crystallites (fig. 6). After melting, the liquidus temperature was checked by manipulating the temperature until a few crystals remained in equilibrium with the melt. This occurred at the reported value of 1020 ± 5° C when two types of crystals could be distinguished: acicular crystals and much finer microcrystals. X-ray analysis of the quenched bead confirmed the two phases to be Li_2SiO_3 and β-spodumene.

Figure 5 Extraction replica of spherulites from which Li_2SiO_3 has been dissolved. The micrograph shows the branched filamental character of the β-eucryptite ss crystallites.

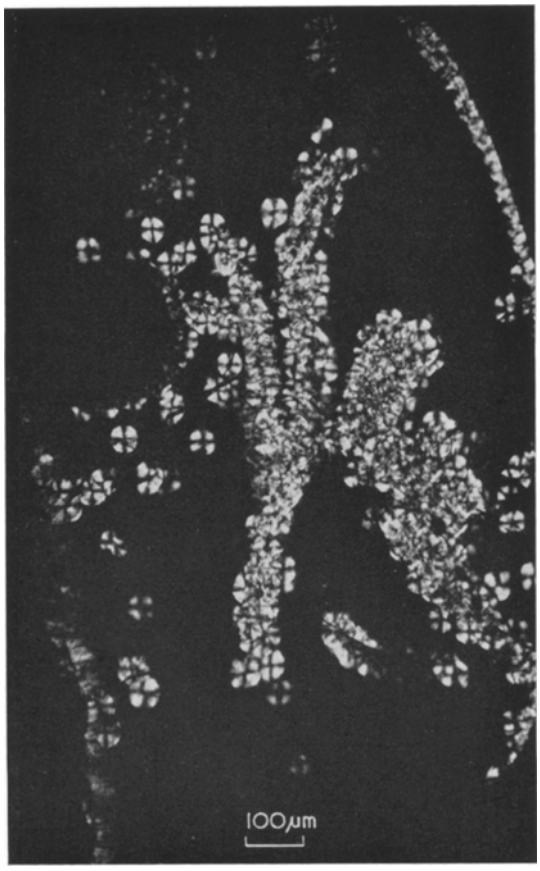

Figure 4 Two phase spherulites of Li_2SiO_3 and β-eucryptite ss. Growing during the early stages of the exothermic effect in G66.

4.2. Observations on G69

During programmed heating between T_g and the crystallisation exotherm the beads of this glass, like those of G66, remained optically clear, and replicas of quenched specimens were similarly featureless in the electron microscope. Beads heated isothermally for 6 h at temperatures in the range 530 to 550° C also remained free of any observable microphase separation. Such heat-treatment however made a noticeable difference in the size and numbers of the growth units crystallising during the exothermic reaction. In this glass the crystals grew with the polyhedral morphology shown in fig. 7 and had a dendritic internal structure based on a well defined spine of β-eucryptite ss from which

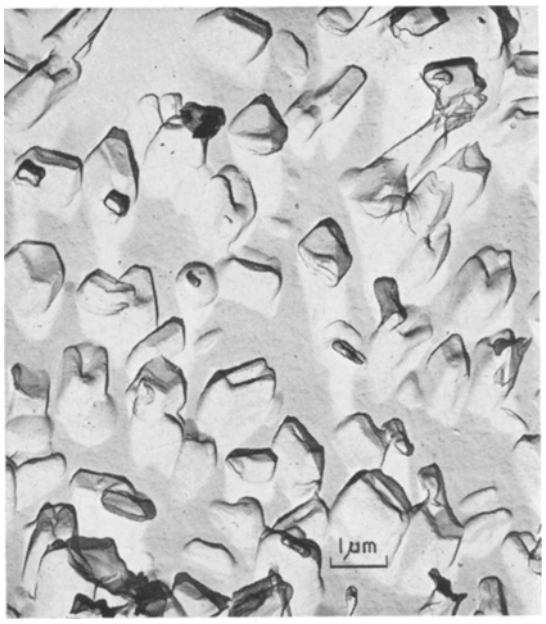

Figure 6 Microstructure of G66 at 900° C. Blocky crystallites of Li_2SiO_3 and β-eucryptite ss recrystallised from spherulitic grains.

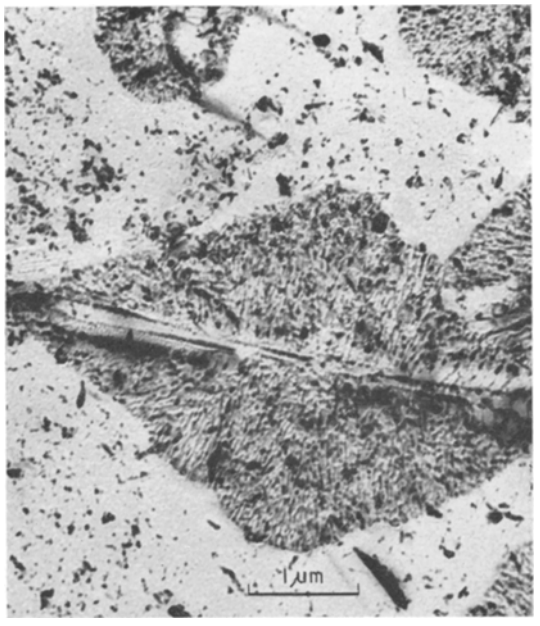

Figure 7 Two-phase (Li_2SiO_3 and β-eucryptite ss) dendrites growing at 750° C during early stages of μDTA of G69. Note the well-defined spine of β-eucryptite ss.

fibrils radiated. Fig. 7 shows these dendrites on a replica taken from a bead quenched at 750° C during DTA. When beads had been preheated for 6 h at 530° C the size at impingement of the units was only $\sim 3\mu$m, i.e. the nucleation density of the glass was of the order 3×10^{10} cc^{-1}. The impingement size, if no preheating were given, was ~ 20 μm, showing the number of nuclei to be reduced more than a hundredfold to $\sim 1 \times 10^8$.

X-ray analysis of beads quenched after the exothermic effect showed lithium metasilicate, β-eucryptite solid solution ($a = 5.19$, $c = 5.43$ Å) and lithium titanate. It has been established that the dendrites maintain the quasi eutectic character found in the spherulites, being similar composite structures of lithium metasilicate and a β-eucryptite solid solution. The orientation relationships between these two phases in the growth units have been worked out [3] from electron diffraction studies on extraction replicas of these units grown in bulk glass. It will be shown later (section 5.1) that the rate of growth of the dendrites is slower than that of the spherulites. Some replicas of beads quenched during the crystallisation showed the presence of star-shaped crystallites (fig. 8), presumed to be lithium titanate, growing near the dendrites.

4.3. Observations on G70

During the early stages of DTA, beads of this glass remained optically clear, X-ray amorphous,

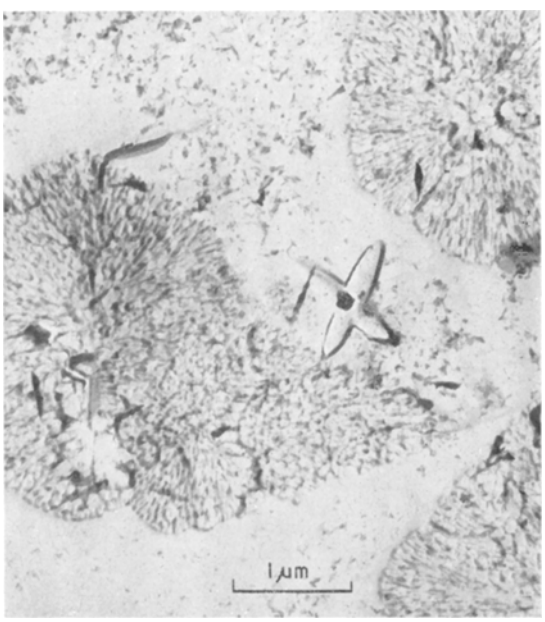

Figure 8 Secondary growth of twinned crystallites, presumably lithium titanate, following primary growth of the dendrites during μDTA of G69.

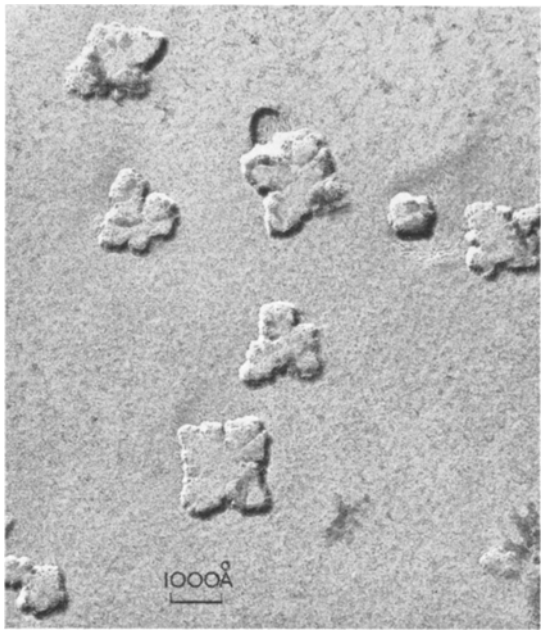

Figure 9 Crystallites of lithium titanate growing just prior to exotherm during μDTA of G70.

and free of any observable microstructure in the electron microscope. A faint opalescence developed at 700° C preceding the exothermic effect (cf. fig. 3c) which occurred at 720° C. Droplets quenched at this point were shown to contain irregular-shaped crystallites (1000 to 2000 Å) of lithium titanate (fig. 9). When beads of this glass were held at 520° C, just above T_g, for 16 h or more, this phase appeared as cubic crystallites ~400 Å in size (figs. 10a and b). An analysis of the micrographs showed that there were approximately 2×10^{15} crystallites per cc, a value almost identical to that found from studies on bulk glass [3].

The sharply resolved heat effect at 720° C coincided with the sudden opacification of the droplet by the swift growth of very fine crystals. Visual observation of the size, shape and rate of growth of the crystals was prevented by the rapidity of crystallisation. The phases present were shown, by X-ray diffraction, to be lithium titanate, lithium metasilicate and a β-eucryptite solid solution.

To follow the development of microstructure during the exothermic period, beads were quenched at successive stages and examined by electron microscopy. It was clear that the three phases were growing as discrete crystallites and were epitaxially unrelated. From fig. 11 and related micrographs it can be inferred that the spherulitic regions are β-eucryptite, the elongated crystals are lithium metasilicate and the cubic species is lithium titanate. Some of the individual character of their morphology is preserved in the

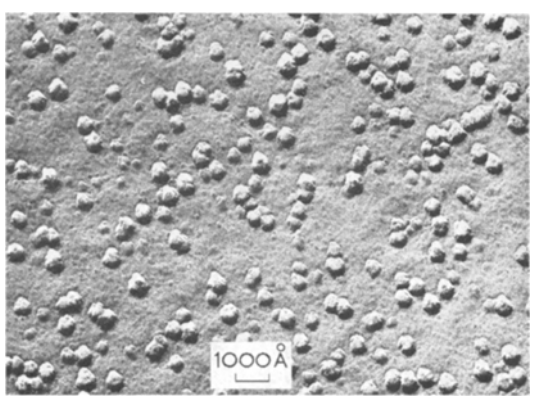

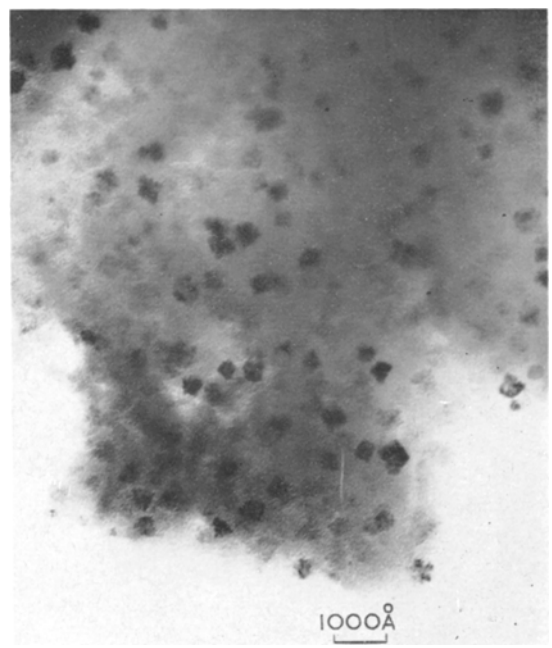

(a) (b)

Figure 10 (a) Replica of crystallites of lithium titanate growing isothermally at 520° C in a microdroplet of G70. (b) Transmission micrograph of a thin section of a bead, showing crystallites (cf. fig. 10a) of lithium titanate growing isothermally at 520° C in G70.

microstructure of the fully crystallised bead. Replicas of the beads at this stage showed them to be fine-grained and to have irregular-shaped internal boundaries (fig. 12).

5. Kinetic Data

In studies on the rate of crystallisation of glasses it is necessary to consider both (a) the rate at which individual crystals grow and, (b) the rate at which the overall volume of the glass is transforming into a crystallised body. Of the three glasses, only G66 and G69 crystallised in such a way that the rate of growth of individual crystals could be measured directly.

The rate of volume crystallisation and the associated Arrhenius plots were obtained for all three glasses by an analysis of the thermograms.

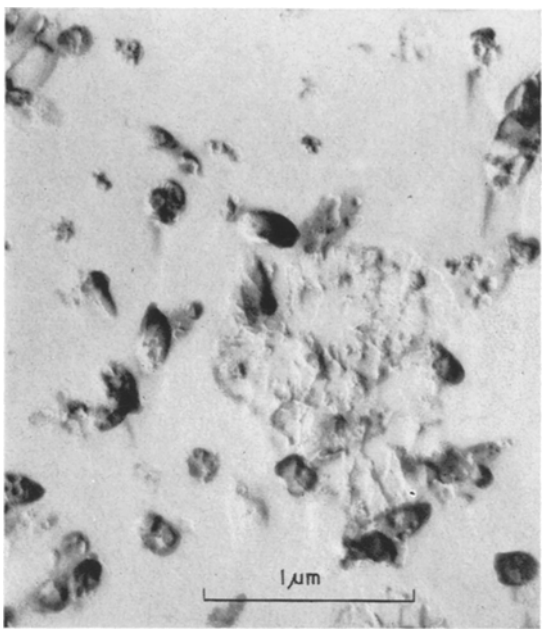

Figure 11 Replica of G70 quenched at an early stage of crystallisation during the exotherm. The figure shows the separate growth of the three phases, Li_2SiO_3, $LiTiO_3$ and β-eucryptite ss.

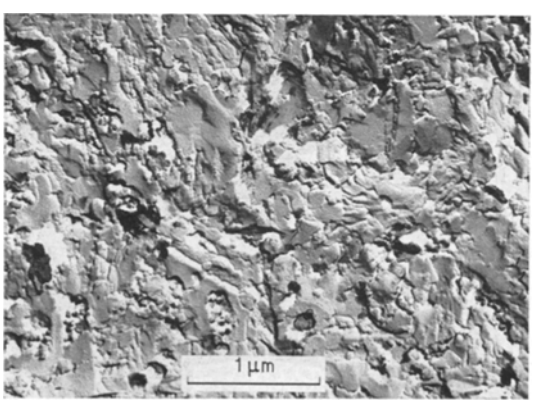

Figure 12 Replica of G70 quenched after completion of the exothermic peak.

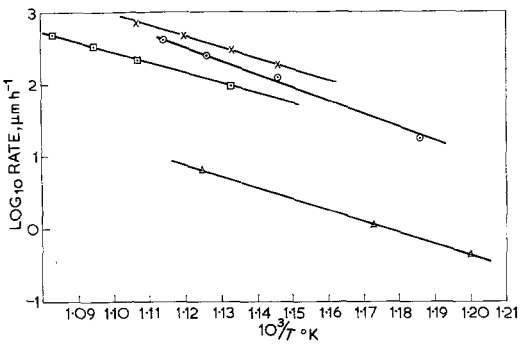

Figure 13 Arrhenius plots of crystal growth rates in G66 and G69. Comparison of data from hot stage microscopy and bulk glass studies. X, G66 (hot stage) activation energy 68 kcal mol^{-1}; ⊙, G66 (bulk glass) activation energy 88 kcal mol^{-1}; ⊡, G69 (hot stage) activation energy 63 kcal mol^{-1}; △, G69 (bulk glass) activation energy 73 kcal mol^{-1}.

5.1. Individual Crystal Growth Rate in G66 and G69

The data is recorded (fig. 13) in the form of Arrhenius plots of the growth rates, which were linear at the temperatures studied until crystal impingement occurred. The data obtained from isothermal studies on bulk quantities of these glasses is also recorded for comparison. Although growth rates in general are shown to be higher in microdroplets, the data confirms that the biconical dendrites in G69 grow more slowly than the spherulites in G66. Both sets of data show that the apparent activation energy of dendrite growth is lower than that for spherulite growth. Activation energies calculated in this way are considered to be a sufficient guide to whether the transformation is controlled by diffusion or viscous flow processes, since there is usually an order of magnitude difference in apparent activation energy between these processes.

5.2. Kinetic Parameters Relating to Volume Crystallisation

Borchardt [8, 9] and Daniels [8] showed that a simple analysis of thermograms could provide values both for the initial rates of reaction and the corresponding activation energies. This treatment was applied to studies on organic reactions and inorganic dehydrations and decarboxylations.

A similar treatment is applied here to determine the initial rate at which a glass crystallises and the apparent activation energy governing the process.

If n_0 is the molar concentration of the crystallising species, then from equation 3 the heat of reaction per mole is

$$\frac{\triangle H}{n_0} = \frac{KA}{n_0}. \tag{9}$$

Since the heat of reaction, $\mathrm{d}\triangle H$, over a small time interval is proportional to the number of moles reacting ($-\mathrm{d}n$) in that time, it follows that

$$\mathrm{d}\triangle H = -KA\frac{\mathrm{d}n}{n_0}. \tag{10}$$

Substituting equation 10 in equation 1 and differentiating with respect to time, we have

$$\frac{-KA}{n_0}\frac{\mathrm{d}n}{\mathrm{d}t} = C_\mathrm{p}\frac{\mathrm{d}\triangle T}{\mathrm{d}t} + K\triangle T, \tag{11}$$

or

$$\frac{-\mathrm{d}n}{\mathrm{d}t} = \frac{n_0}{KA}\left(C_\mathrm{p}\frac{\mathrm{d}\triangle T}{\mathrm{d}t} + K\triangle T\right), \tag{12}$$

which expresses the reaction rate at any temperature in terms of the slope ($\mathrm{d}\triangle T/\mathrm{d}T$) and height from base line ($\triangle T$) of a DTA peak.

In a typical thermogram using 500 μg of a glass in our apparatus $\mathrm{d}\triangle T/\mathrm{d}t = 1^\circ$ C sec^{-1} and $\triangle T = 10^\circ$ C. Since $K = 0.45$ mcal $^\circ$C^{-1}sec^{-1} and $C_\mathrm{p} \sim 0.17$ mcal $^\circ$C^{-1}, then $C_\mathrm{p}(\mathrm{d}\triangle T/\mathrm{d}t) = 0.17$ mcal sec^{-1}, whereas $K\triangle T = 4.5$ mcal sec^{-1}. Therefore, to a first approximation $C_\mathrm{p}(\mathrm{d}\triangle T/\mathrm{d}t)$ can be neglected and equation 12 reduces to

$$\frac{-\mathrm{d}n}{\mathrm{d}t}\frac{1}{n_0} = \frac{\triangle T}{A}, \tag{13}$$

which relates the rate of reaction, expressed as the fraction reacting in unit time, to the ratio of the peak height to the area at a given temperature.

Since DTA peaks usually approximate to triangles (cf. fig. 3) it follows from equation 13 that

$$\frac{-\mathrm{d}n}{\mathrm{d}t}\frac{1}{n_0} = \frac{2\triangle T}{B\triangle T_\mathrm{max}}, \tag{14}$$

where B is the length of the base of the peak expressed in units of time.

Table II includes crystallisation rates at 750° C calculated in this way for the three glasses. The overall rates of volume crystallisation are in the order G66 < G69 < G70.

Since the general rate equation is of the form

$$\frac{-\mathrm{d}n}{\mathrm{d}t}\frac{1}{n_0} = Z\mathrm{e}^{-E/RT}f(\alpha) \tag{15}$$

where Z is a frequency factor, E is the activation energy, and $f(\alpha)$ a function of the dependence of the reaction rate on concentration of reacting species and order of reaction, it follows from equation 13 that

$$\ln\triangle T = \mathrm{const} + \ln f(\alpha) - \frac{E}{RT}. \tag{16}$$

If $f(\alpha)$ is small, i.e. the reaction is first order or less, then Arrhenius plots of $\ln\triangle T$ vs $1/T$ will be linear and apparent activation energies can be directly derived from the thermograms. This method was used by Piloyan, Ryabchikov and Novikova [10] to derive activation energies for the dehydration and decarboxylation of several inorganic salts. The agreement between results produced in this way and those from more conventional methods was excellent.

In the present study it was found that such Arrhenius plots from the thermograms of the glasses were in fact linear and good agreement was found between values of the apparent activation energy calculated from different thermograms of a given glass. Typical plots are shown in fig. 14 and the apparent activation energy values are included in table II. These activation energies are not necessarily related to those previously calculated from the rate of radial growth of individual spherulites since here we are considering volume rate of crystallisation.

The method of Borchardt and Daniels [8] for the derivation of activation energies from thermograms has been the subject of discussion elsewhere but its general validity has gained support. Reed, Weber and Gottfried [14], for example, showed that thermograms which agree well with experimental curves, can be generated by numerical integration of the equations. The criticisms of Garn [15] of this approach relate mainly to geometry and sample siting factors, which in conventional DTA gives rise to

temperature non-uniformity. In the present μDTA arrangement the temperature uniformity is closer to that which held in Borchardt and Daniel's stirred liquid system.

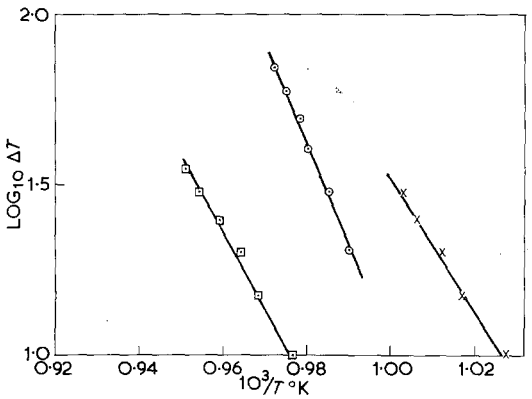

Figure 14 Apparent activation energies of volume crystallisation derived from thermograms. X, G66 activation energy 87 kcal mol^{-1}; □, G69 activation energy 100 kcal mol^{-1}; ○, G70 activation energy 139 kcal mol^{-1}. Heating rate 3.6° C sec^{-1}.

6. Discussion

Since the purpose of this communication is to draw attention to the scope of the technique, the results used as illustrations will not be discussed at any length. The crystallisation behaviour of the three glasses has in any case been fully described in a previous communication [3].

The rapid determination of reaction temperatures, crystal morphology, individual crystal growth rates and rates of volume crystallisation in relation to well defined thermal history is particularly relevant when exploring the processes of producing glass-ceramics [11]. With the associated information from X-ray diffraction and electron microscopy, the present hot stage technique has an obvious application to studies on such materials, with the exception of volatile systems (e.g. fluoride-containing melts). In its capacity to produce structural data this technique is seen as a supporting method to bulk quantity studies.

The usefulness of applying the apparatus, as a simple hot stage microscope, to studies on equilibrium phase relationships and to the determination of individual crystal growth rates has been made clear in previous publications [12, 13].

The significance of the activation energies of crystallisation processes is still not clear. However, tentative conclusions can sometimes be made about rate-controlling processes. For example, Degen and Toropov [16] found that in a Li_2O-SiO_2 glass in which the activation energy of diffusion of Li^+ ions was 19 kcal mol^{-1} and that of O^{2-} ions 32 kcal mol^{-1}, spherulites grow with an activation energy of 50 kcal mol^{-1}. Similarly the activation energy of spherulite growth in a Na_2O-SiO_2 glass was 85 kcal mol^{-1}, the corresponding activation energies for Na^+ and O^{2-} diffusion being 13 kcal mol^{-1} and 53 kcal mol^{-1} respectively.

It was concluded from these data that the crystal growth was governed by the movement of "complexes" rather than simple ions. Viscous flow, for which activation energies are usually high, also presumably depends on the movement of such complexes. Pure silica, for example, has an activation energy of viscous flow of between 180 and 140 kcal mol^{-1} over the range 1710 to 1900° C [18].

In the lithium aluminosilicate glasses studied in the present work it appears that the activation energies are nearer to those expected for the movement of three-dimensionally bonded flow units than for the migration of simple ions. These apparent activation energy values and the rates of volume crystallisation are clearly sensitive to the ionic ratios of $Li^+ : Al^{3+} : Si^{4+} : Ti^{4+}$. This has been discussed elsewhere [3]. Since it cannot always be expected that crystallisation will follow a single rate expression, any meaningful interpretation of activation energies must await more data.

In a new instrumental development by Sommer [17] a balanced temperature analyser has been described which records the energy required to keep $\triangle T = 0$ between the two thermocouples. Heat flow problems, the most difficult to formalise in DTA, should be eliminated since the direct recording of heats of reaction removes calibration errors. This device may well add to the power of μDTA methods in the exploration of high temperature behaviour.

Acknowledgement

The authors wish to thank Dr T. I. Barry for helpful discussions during the course of this work and for his constructive criticisms of the text.

References

1. P. D. GARN, "Thermoanalytical Methods of Investigation" (Academic Press, New York & London, 1965) p. 149.
2. R. P. MILLER and G. SOMMER, *J. Sci. Instr.* **43** (1966) 293.

3. T. I. BARRY, D. CLINTON, L. A. LAY, R. A. MERCER, and R. P. MILLER, *J. Mater. Sci.* **4** (1969) 596.
4. J. H. WELCH, *J. Sci. Instr.* **31** (1954) 458.
5. R. A. MERCER and R. P. MILLER, *ibid* **40** (1963) 352.
6. L. GLASSER and R. P. MILLER, *J. Chem. Ed.* **42** (1965) 91.
7. C. MAZIÈRES, *Analyt. Chem.* **36** (1964) 602.
8. H. J. BORCHARDT and F. DANIELS, *J. Amer. Chem. Soc.* **79** (1957) 41.
9. H. J. BORCHARDT, *J. Inorg. Nucl. Chem.* **12** (1960) 252.
10. G. O. PILOYAN, I. D. RYABCHIKOVA, and O. S. NOVIKOVA, *Nature* **212** (1966) 1229.
11. P. W. MCMILLAN, "Glass Ceramics" (Academic Press, New York & London, 1964).
12. W. GUTT, *Silicates Industriels* **27** (1962) 285.
13. D. BURNETT, D. CLINTON, and R. P. MILLER, *J. Mater. Sci.* **3** (1968) 47.
14. L. R. REED, L. WEBER, and B. S. GOTTFRIED, *Ind. and Eng. Chem. (Fundamentals)* **4** (1965) 38.
15. [1] p. 196.
16. M. G. DEGEN and N. A. TOROPOV, *Izvest. Akad. Nauk SSSR Neorg. Mat.* **2** (1966) 1617.
17. G. SOMMER and H. W. SANDER, 2nd Intern. Conference Thermal Analysis, Worcester, Mass. USA, 1968.
18. J. D. MACKENZIE, "Modern Aspects of the Vitreous State" (Butterworths, London, 1960) p. 190.

Received 13 July and accepted 25 August 1969.

Letters

Electron Microscopic Observations on the Phase Transformation in Sintered Iron Disilicide

Iron disilicide possesses a tetragonal metallic high-temperature modification (α-phase) and a semiconducting low-temperature phase (β-phase) with orthorhombic lattice structure [1-4]. According to the phase diagram [5] the β-phase can be formed by a solid state reaction, described in [5], during heat-treatment in its stability range. So far [5-8] the phase transformation has been investigated using the following methods: dilatometry, electrical conductivity, X-ray analysis and the change of the magnetic susceptibility. Using these integrating methods, however, different time characteristics for the phase transformation are obtained (fig. 1) due to the varying effect of additional phases [5], which participate in the transformation, on the physical properties investigated here. Since the grain-size in sintered material is small (some μm) it is difficult to detect details by optical observation. Therefore it was of interest to observe the phase change by electron-microscopic transmission. For this purpose the preparation of pure and differently doped $FeSi_2$ was carried out according to [9]. The doping concentrations were 2 at. % aluminium (p-type conduction) and 5 at. % cobalt (n-type conduction), respectively. These materials have practical importance for thermoelectric applications [10, 11].

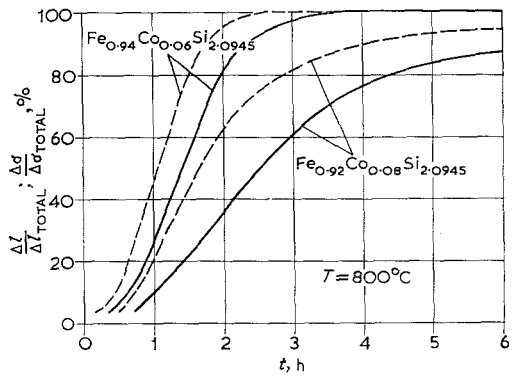

Figure 1 Length change $\Delta l/\Delta l_{total}$ (solid lines) and electrical conductivity change $\Delta\sigma/\Delta\sigma_{total}$ (dashed lines) during phase transition.

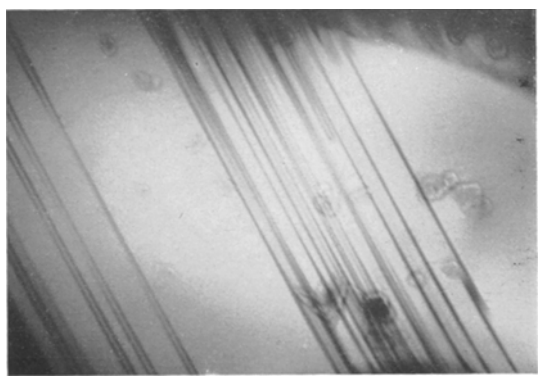

Figure 2 Lamellar structures in the low-temperature phase (× 73 300).